

Transformation-induced plasticity in an ultrafine-grained steel: An *in situ* neutron diffraction study

Kaixiang Tao, Hahn Choo,^{a)} and Hongqi Li

Department of Materials Science and Engineering, The University of Tennessee, Knoxville, Tennessee 37996

Bjørn Clausen

Los Alamos Neutron Science Center, Los Alamos National Laboratory, Los Alamos, New Mexico 87545

Jae-Eun Jin and Young-Kook Lee

Department of Metallurgical Engineering, Yonsei University, Seoul 120-749, Republic of Korea

(Received 12 October 2006; accepted 31 January 2007; published online 8 March 2007)

An ultrafine-grained steel with an average grain size of about 350 nm was developed. The tensile testing at ambient temperature shows a threefold increase in the yield strength compared to its coarse-grained counterpart. Moreover, the increase in the strength was achieved without the sacrifice of the ductility due to strain-induced martensitic transformation. The evolution of lattice strains and phase fractions of the austenite and martensite phases during the deformation was investigated using *in situ* neutron diffraction to provide a micromechanical understanding of the transformation-induced plasticity responsible for the combination of high strength and ductility.

© 2007 American Institute of Physics. [DOI: 10.1063/1.2711758]

Nanocrystalline and ultrafine-grained (UFG) materials have received extensive attention in recent years.¹ It is well known that the strength can be dramatically enhanced by reducing the grain size based on the Hall-Petch relationship. However, the high yield strength is usually achieved at the expense of the ductility as there is little uniform elongation after yielding due to the lack of strain hardening.² The strain hardening process is typically associated with the accumulation and interaction of the dislocations. However, the UFG metals usually have a high initial dislocation density, which is introduced during the processing of the material through the severe plastic deformation. Therefore, the saturation of the dislocation density results in very low strain hardening rate during subsequent deformation and hence poor ductility.²

However, in the case of the recently developed UFG transformation-induced plasticity (TRIP) steel,³ the martensitic phase transformation provides an effective source of strain hardening. The replacement of the austenite by the much harder martensite phase increases the strain hardening rate and delays the strain localization. The prevention of premature necking leads to a significant increase in the uniform elongation. Meanwhile, the transformation strains (volume and shear strains) that accompany the phase transformation also contribute to the ductility improvement. In this letter, we present the experimental results of the *in situ* neutron diffraction studies to provide micromechanical insights to the transformation and deformation behavior of the UFG TRIP steel.

The material selected for this study is the Fe–Cr–Ni–Mn steel with a nominal composition (in wt %) of 10% Cr, 5% Ni, 8% Mn, 0.1% C, and balance Fe. The ingot was hot rolled to a 10-mm-thick plate and was solution treated at 1473 K for 30 min. The solution-treated plate was cold rolled with about 75% thickness reduction, and most of the γ (fcc) phase was transformed into the α (bcc) phase. Then, the

plate was annealed at 913 K for 10 min to induce the reverse transformation of the mechanically induced α back to γ . After the reverse transformation, the UFG austenite (γ) was obtained. Figure 1 shows the transmission electron microscopy (TEM) image of the UFG steel sample, which exhibits well-defined grain boundaries and an average grain size of about 350 nm. A more detailed description of the material preparation is available in the literature.³

The room-temperature tensile tests and *in situ* neutron diffraction measurements were performed on two different specimens using the SMARTS instrument at Los Alamos Neutron Science Center:⁴ (1) Coarse-grained (CG) steel, the solution-treated (50 μm) specimen, and (2) UFG steel, the cold-rolled/annealed (350 nm) specimen. The *in situ* neutron diffraction spectra were recorded as a function of the applied stress during the tensile tests. At SMARTS, the tensile loading axis is oriented at 45° relative to the incident neutron beam with the scattering angle fixed at $2\theta = \pm 90^\circ$ for two detector banks. This scattering geometry allows the simultaneous measurements of the lattice strains parallel (axial) and perpendicular (transverse) to the tensile axis. The phase frac-

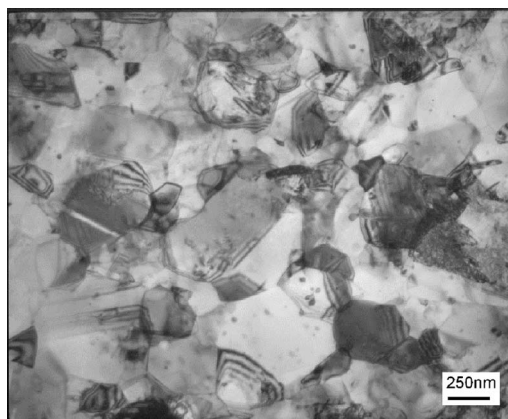


FIG. 1. TEM bright field image of the UFG TRIP steel. The average grain size is about 350 nm.

^{a)} Author to whom correspondence should be addressed; electronic mail: hchoo@utk.edu

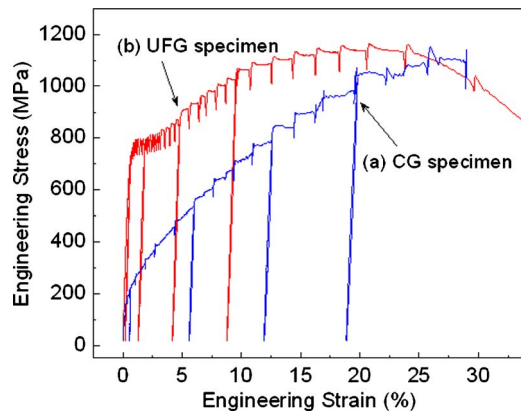


FIG. 2. Tensile stress-strain curves of (a) coarse-grained (CG) steel with an average grain size of $50\ \mu\text{m}$ and (b) ultrafine-grained (UFG) steel with an average grain size of $350\ \text{nm}$.

tion and the lattice strain are determined by the Rietveld analysis using the general structure analysis system.⁵ More details about the *in situ* neutron diffraction measurements and data analysis can be found in the literature.^{6–8}

The macroscopic tensile stress-strain curves recorded during the *in situ* neutron diffraction measurements are presented in Fig. 2. The serrations (load drops) are due to the stress relaxation that occurred while holding the specimen at a constant displacement (for about 20 min) for the measurement of diffraction pattern. A few unloads were also performed to measure the residual lattice strains (not discussed here). The UFG steel shows a yield stress of about 730 MPa, which is dramatically higher than that of the CG steel (about 210 MPa) mainly due to the grain refinement. On the other hand, the uniform elongation of the UFG steel (20%) is close to that of the CG steel (25%); that is, the strength is improved markedly without a significant loss of the ductility.

Figure 3 shows the (a) weight fraction evolution and (b) lattice strain evolution of the three phases (γ -fcc austenite, α -bcc, and ϵ -hcp martensites) in the solution-treated CG steel as a function of the applied stress. Before loading, all three phases appear in the undeformed sample; in the elastic regime, no weight fraction changes were observed. When the elastic limit (σ_E , about 125 MPa) is reached, the result clearly shows the strain-induced martensitic transformation, where the metastable fcc phase transforms to the bcc phase. The fcc to bcc transformation is accomplished by a combination of the lattice deformation, simple shear, and rigid body rotation.⁹ The bcc phase fraction starts to increase at the very beginning of the plasticity, and the increase becomes quite linear after the yield point (σ_y , about 210 MPa). For the hcp martensite, the phase fraction increased at the early stage of the plastic deformation and then decreased along with the significant reduction in the amount of the fcc phase. The martensitic transformation, which involves both ϵ and α phases, is often observed to occur in the sequence of $\gamma \rightarrow \epsilon \rightarrow \alpha$, and the ϵ phase is believed to be an intermediate phase.^{10,11}

The martensite formation plays an important role in the internal stress development. From Fig. 3(b), it is seen that the strain responses (along the loading direction) of the fcc austenite and the hcp martensite are qualitatively similar and both deviate towards lower lattice strain from the linearity at about 400 MPa (the dashed lines are the linear fits of the elastic responses of fcc and bcc phases), indicating the com-

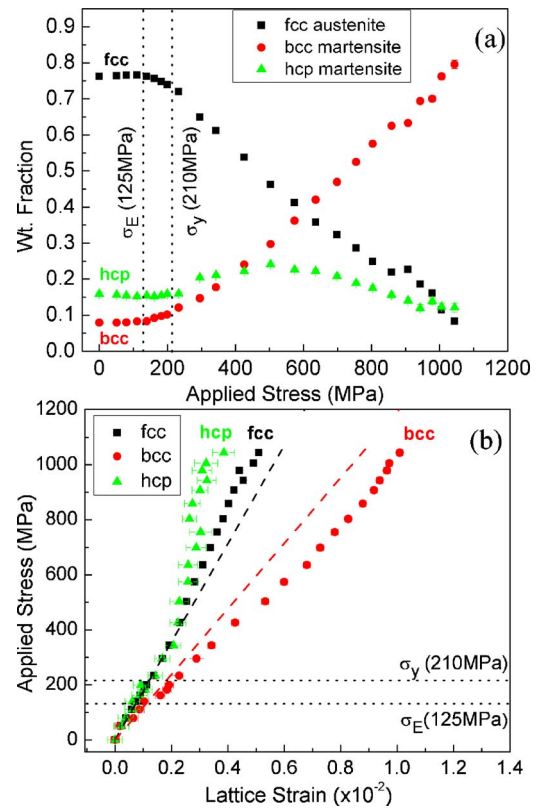


FIG. 3. Evolution of the weight fraction (a) and axial lattice strain (b) of austenite and martensite phases in the coarse-grained (CG) steel during the room-temperature tensile testing. (σ_E -elastic limit; σ_y -0.2% yield stress).

pressive internal stresses developing in these two phases.¹² On the other hand, the bcc martensite deviates to the larger lattice strain after yielding, and the tensile internal stress is generated in this phase. With the macroscopic applied stress increasing and the bcc phase fraction increasing linearly, the bcc martensite shares the applied load and plays a role in strengthening. Accordingly, a significant hardening effect can be observed in the CG sample, as shown in Fig. 2.

Figure 4 shows the (a) weight fraction evolution and (b) lattice strain evolution in the UFG steel as a function of the applied stress. In this case, the hcp phase was not included in the Rietveld analysis due to its very small amount (less than 5 wt %) and broad peak profile. In comparison to the CG steel, there are two main differences: (1) the initial bcc phase fraction is much smaller due to the reverse transformation, and (2) the transformation is “rapid” once the applied stress reaches σ_y (730 MPa), followed by a gradual increase above 765 MPa. The rapid increase in the amount of the bcc phase, which may be due to the higher stress status when the plastic deformation starts, is consistent with the appearance of the short plateau observed in the macroscopic stress-strain curve of the UFG steel.

The large error bar presented in the bcc lattice strain response [Fig. 4(b)] is due to the uncertainty in the initial lattice parameter (a_0) of the small amount of the bcc phase. (The lattice strain data are calculated relative to the a_0 .^{7,8}) Also, due to the large uncertainty in the bcc lattice strain in the elastic region, it is difficult to identify the accurate stress level where the lattice strain of the bcc martensite starts to deviate significantly from the linearity. However, it is evident that a large tensile lattice strain starts to develop at about 600 MPa. The rapid development in the lattice strain of the

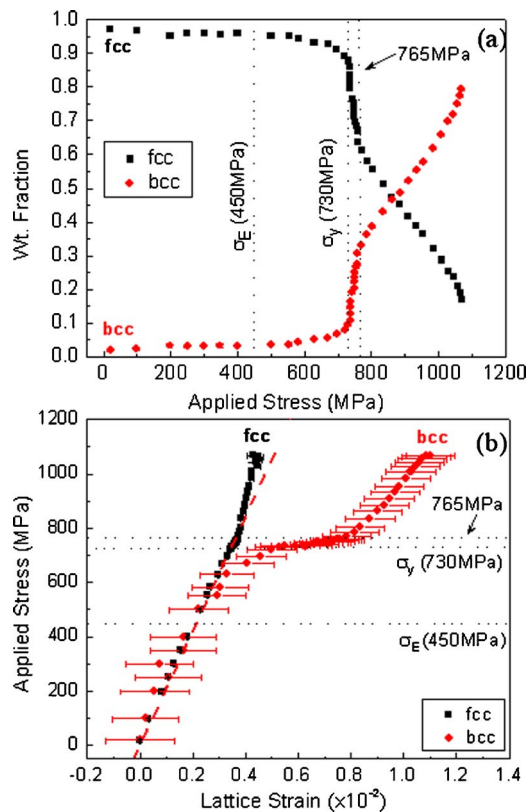


FIG. 4. Evolution of the weight fraction (a) and axial lattice strains (b) of fcc austenite and bcc martensite phases in the UFG steel during the tensile testing.

bcc phase is caused by the partitioning of the applied load from the fcc matrix phase to the bcc phase with a small initial phase fraction. After the rapid martensite formation between 730 and 765 MPa [Fig. 4(a)], the internal stress development in the martensite starts to slow down from about 765 MPa since more bcc phases start to share the load. On the contrary, the austenite phase shows a relatively linear response although a small deviation above 765 MPa can be observed. It seems that the compressive internal stress in the fcc phase starts to develop only after the fraction of the bcc phase becomes appreciable.

There are two deformation modes operating in the TRIP steel during the tensile deformation: transformation straining due to the deformation-induced martensite formation and plastic deformation (slip) by the dislocation motion.^{13–15} The rapid martensite formation [Fig. 4(a)] and the plateau in the stress-strain curve (Fig. 2) indicate that the transformation strain is the dominant source of deformation at the early

stage of the plastic deformation in the UFG TRIP steel. Most of the elongation in the plateau region may come from the transformation strain. The dislocation slip in fcc contributes relatively little to the total elongation at this stage, and there is no (or very little) plastic deformation in the newly formed martensite. Therefore, no strain hardening can be observed although the much stronger bcc martensite phase rapidly forms. When the martensite formation slows down, the plateau in the stress-strain curve ends. The deformation changes to a mixed mode of transformation and dislocation motion, and the hardening behavior, which plays an important role in stabilizing the plastic flow, becomes apparent.

In summary, the strain-induced phase transformation behavior in an ultrafine-grained TRIP steel was investigated using *in situ* neutron diffraction. The martensite formation and the concurrent load partitioning between the austenite and the newly forming martensite phases were identified as the source of the strain hardening that facilitates the high ductility maintained in the UFG steel.

This work is supported by the NSF International Materials Institutes (IMI) Program under DMR-0231320. This work has benefited from the use of the Los Alamos Neutron Science Center (LANSCE) at the Los Alamos National Laboratory. LANSCE is funded by the U.S. Department of Energy under Contact No. W-7405-ENG-36.

¹R. Z. Valiev, R. K. Islamgaliev, and I. V. Alexandrov, *Prog. Mater. Sci.* **45**, 103 (2000).

²Y. M. Wang and E. Ma, *Acta Mater.* **52**, 1699 (2004).

³Y. Q. Ma, J. E. Jin, and Y. K. Lee, *Scr. Mater.* **52**, 1311 (2005).

⁴M. A. M. Bourke, D. C. Dunand, and E. Ustundag, *Appl. Phys. A: Mater. Sci. Process.* **74**, S1707 (2002).

⁵R. B. Von Dreele, J. D. Jorgensen, and C. G. Windsor, *J. Appl. Crystallogr.* **15**, 581 (1982).

⁶H. Choo, M. Bourke, P. Nash, M. Daymond, and N. Shi, *Mater. Sci. Eng., A* **264**, 108 (1999).

⁷B. Clausen, T. Lorentzen, M. A. M. Bourke, and M. R. Daymond, *Mater. Sci. Eng., A* **259**, 17 (1999).

⁸H. Choo, D. Seo, J. Beddoes, M. A. M. Bourke, and D. W. Brown, *Appl. Phys. Lett.* **85**, 4654 (2004).

⁹C. M. Wayman, *Introduction to the Crystallography of Martensitic Transformations* (Macmillan, New York, 1964), p. 92.

¹⁰R. Lagneborg, *Acta Metall.* **12**, 823 (1964).

¹¹J. A. Venables, *Philos. Mag.* **7**, 35 (1962).

¹²E. C. Oliver, P. J. Withers, M. R. Daymond, S. Ueta, and T. Mori, *Appl. Phys. A: Mater. Sci. Process.* **74**, 1143 (2002).

¹³G. L. Huang, D. K. Matlock, and G. Krauss, *Metall. Trans. A* **20A**, 1239 (1989).

¹⁴S. S. Hecker, M. G. Stout, K. P. Staudhammer, and J. L. Smith, *Metall. Trans. A* **13A**, 619 (1982).

¹⁵G. B. Olson, in *Deformation Processing and Structure*, edited by G. Krauss (ASM, Metals Park, OH, 1984), p. 391.